Astron. Astrophys. 325, 782–790 (1997)

ASTRONOMY
AND
ASTROPHYSICS

# Determination of the length of coronal loops from the decay of X-ray flares

## I. Solar flares observed with Yohkoh SXT

**F. Reale**[1], **R. Betta**[1], **G. Peres**[1], **S. Serio**[1], **and J. McTiernan**[2]

[1] Istituto e Osservatorio Astronomico, Piazza del Parlamento 1, I-90134 Palermo, Italy
[2] Space Sciences Lab., Univ. of California, Berkeley, USA

Received 9 December 1996 / Accepted 21 March 1997

**Abstract.** We show how to estimate the size of spatially unresolved solar and stellar coronal flaring regions from the X-ray light curve and time-resolved temperature and emission measure values during the flare decay. By means of extensive hydrodynamic modeling of decaying flaring loops, we propose and test a relationship between the decay time of the light curve in the band of a specific instrument and the slope of the trajectory in the density-temperature diagram. From this relationship, we obtain an expression of the loop length as a function of the decay time, the slope and the flare maximum temperature. The novelty of this approach is that it takes into proper quantitative account, and allows us to estimate, the effect of a prolonged heating during the decay. In view of its application to non-imaged solar flares and to stellar flares, we have tested our relationship on spatially resolved solar flares observed with Yohkoh SXT. The comparison of the predictions to the morphology of the structures in the SXT images proves the reliability of our approach under a wide range of conditions.

**Key words:** Sun: flares – Sun: corona – stars: coronae – stars: flares

### 1. Introduction

It is widely accepted that solar and stellar X-ray flares share common general features. Flares detected on stars by Einstein, EXOSAT and ROSAT evolve on time scales comparable to those of intense solar flares, and their light curves are similar (e.g. Haisch et al. 1995), although the stellar flares detected are, on the average, brighter and more energetic. This analogy suggests that we interpret stellar flare observations in the light of our more direct and detailed knowledge of solar flares, and assume that all of them are governed by the same basic physical mechanisms.

*Send offprint requests to*: F. Reale

Solar X-ray flares occur inside closed coronal structures, where the plasma is confined by the magnetic field and which often maintain their geometry unaltered for most of the event (e.g. Pallavicini et al. 1977). The general features of such flares can be accounted for by one-dimensional hydrodynamic models which consider a sudden release of thermal energy in the otherwise steady atmosphere confined in a semicircular loop of constant cross-section (Pallavicini et al. 1983).

At the beginning of the decay, flaring loops appear to be close to a steady loop configuration (as discussed in more detail below). During the decay, the temperature is so high, and the thermal conduction so effective, that the spatial distribution of the heating is virtually irrelevant (Serio et al. 1991). While on the one hand this implies that the decay phase can hardly be used to obtain diagnostics of the heating location, on the other hand it allows us to study other properties of flaring loops separating them from the details of the heat deposition.

It is widely accepted that the decay time of flare X-ray light curves is related to the length of the flaring loop (e.g. Haisch 1983, Reale et al. 1988, Serio et al. 1991, Van den Oord et al. 1988): the longer the loop, the longer its decay time. This property has been used to infer the spatial size of unresolved stellar flares. However, if a significant amount of heating is present during the flare decay, it will prolong the decay, and overlooking such a possibility would lead to overestimate the loop length (Reale et al. 1988). In other words the analysis of the light curve cannot provide but an upper limit of the loop length.

For a reliable estimate of the loop length from the flare decay, we need an additional and independent diagnostic of the heating time scale during the decay. Since it has been shown (Jakimiec et al. 1992, Sylwester et al. 1993, Reale et al. 1993) that the slope of the trajectory of the flare decay in the density-temperature ($n$-$T$) plane depends significantly on the heating decay time, and much less on other characteristic parameters such as the loop length, the plasma temperature and pressure (Jakimiec et al. 1992), our strategy will be to use this slope to derive the heating decay time, so to better constrain the loop length.

Under the assumption that flares occur simultaneously inside similar coronal loops with constant cross-section, combining the diagnostics coming from the light curve and from the $n$-$T$ diagram, we have therefore derived a reliable way to estimate the length of the flaring loop. At the same time we are able to constrain the heating time scale during the decay. The tool we have developed promises to be important in studying flares observed with instruments unable to resolve the emitting loops, i.e. stellar flares, but also solar flares observed with non-imaging instruments such as the Bragg Crystal Spectrometer (BCS) on board Yohkoh.

The key point has been to find a relationship linking the decay time of the light curve to the slope of the trajectory in a generalized $\overline{n}$-$T$ diagram, where $\overline{n}$ is the square root of the emission measure[1], i.e. to the heating decay time, as described in more detail in Sect. 3.1. This is a conceptually simple operation. However, the flare light curve results from the evolution of emitting plasma and from the instrument spectral sensitivity. Therefore a quantitative calibration of this relationship has required extensive hydrodynamic modeling of decaying flaring loops with various dimensions and heating time scales, and the synthesis of the flare luminosity from the model results, folding the loop emission through the spectral response of instrument of interest. We have then analysed the light curve and derived the density-temperature evolution as we would do from real data, finally deriving an empirical expression for the loop length as a function of the light curve decay time, of the slope in the $\overline{n}$-$T$ diagram and of the flare temperature. These three quantities are all directly measurable from data, provided that the detector has enough sensitivity and a moderate spectral resolution.

The approach is general and, in principle, applicable to any coronal instrument. The values of the parameters of the expression relating the loop length to the observable quantities depend on the spectral response of the instrument used: we will therefore describe the details considering a specific instrument.

A good way to test the model predictions is to apply it to flares occurring in resolved solar structures, comparing the results to the loop length measured on X-ray images. For this purpose, we have first calibrated it for solar flares observed with the Soft X-ray Telescope (SXT, Tsuneta et al. 1991) on board Yohkoh. This is an imaging wide-band instrument which resolves the flaring loops down to 2.5 arcsec and provides light curves as well as diagnostics of temperature and density, by means of observations through different filters.

Our results make us confident of the validity of the approach, showing that an accurate determination of the flaring loop length cannot neglect the presence of heating during the decay. In this sense our approach makes important progress with respect to others previously adopted. Estimates of the loop length were made in the past using characteristic conductive and radiative cooling times (Haisch 1983), or a combination of them (Reale et al. 1988) with additional complications such as different loop geometries (van den Oord et al. 1988). A recently developed method is based on the combination of the flare rise and decay time (Metcalf & Fisher 1996). All of them neglect the possible influence of additional heating during the decay. An attempt has been made recently to take heating into account just as a free parameter (Graffagnino et al. 1995), studying the space of possible solutions, but with little possibility of discriminating among them. Our approach, instead, provides a single value of loop length, with an error bar mainly due to instrumental uncertainties and to the uncertainties in fitting the trajectory in the $\overline{n}$-$T$ diagram.

In Sect. 2, we describe the model assumptions and the hydrodynamic code used; in Sect. 3 we derive the expression relating the loop length to the light curve decay time and the $\overline{n}$-$T$ slope; in Sect. 4 we show the results of tests of self-consistency and the application to solar flares observed with Yohkoh SXT. In Sect. 5 we summarize and draw our conclusions.

## 2. Loop modeling

Our working hypotheses are that flares occur inside closed coronal loops anchored to the photosphere, that plasma is confined inside each loop, and that its bulk motion and energy transport occur only along the magnetic field lines. We, in particular, assume that the loops are semicircular and symmetric with respect to their apex, have uniform cross-section and maintain their geometry unaltered during the whole flare. We do not pretend that these assumptions are applicable to all X-ray flares, but we believe that they represent a reasonable approximation for the global description of many events.

We therefore describe the plasma evolution using 1-D hydrodynamics of a compressible fluid, taking into account gravity (solar in this case), viscosity, radiative losses and thermal conduction. We use the new Palermo-Harvard hydrodynamic code, with adaptive grid and high resolution even in the very thin and rapidly moving transition region (Betta et al. 1997).

The flare X-ray light curves are normally characterized by a fast rising phase followed by a slower decay phase. Since we are interested in the decay phase, independently of how plasma evolves during the rising phase, we assume that the decay starts after the loop has had enough time to reach quasi-steady conditions, i.e. when energy and plasma flows are negligible. This appears to be the case for many observed flares, as shown by the leveling of the trajectories in the $n$-$T$ diagram (Sylwester et al. 1993). We model the decay of the flaring loops starting from flare maximum conditions and switching off, either abruptly or gradually with an exponential decay, the heating which brought the loop to flaring conditions (Jakimiec et al. 1992, Sylwester et al. 1993). We also assume that the heating is uniformly distributed along the loop. This assumption is not a strong one given the effectiveness of thermal conduction in flare conditions.

In order to map a well representative parameter space, we have computed the evolution of plasma during the flare decay in loops of various semilengths $L$ and different e-folding times $\tau_H$ of the decaying heat release, as listed in more detail in the next section. The next step has been to use the model results, i.e. density, temperature, and velocity distributions along the

[1] $\overline{n}$ is, therefore, proportional to the average density for flares whose volume does not change as in the cases shown.

loop vs time, to synthesize the emission and fold it through the spectral response of the selected instrument. We consider here Yohkoh/SXT, and, in particular, we synthesize the emission $\mathscr{S}_i$, i=1,2 of half-loop per unit time in the bands of the two filters typically used in flare mode observations, Be 119 $\mu$m (i=1) and Al 11.4 $\mu$m (i=2):

$$\mathscr{S}_i(t) = \mathscr{A} \int_0^{s_{max}} n^2(s,t) G_i(T(s,t)) ds \quad (1)$$

where $\mathscr{A}$ is the loop cross-section area (assumed a circle with diameter 1/10 of the loop length), $n$, $T$ are the plasma number density and temperature, $G_i(T)$ ($i$ = 1, 2) is the plasma emissivity folded through the instrumental response per unit emission measure with each of the filters[2], $s$ is the field line coordinate along the loop and $t$ is the time, $s_{max}$ is the location of the loop apex.

From the ratio $\mathscr{S}_1/\mathscr{S}_2$ of the light curves we derive the evolution of the effective temperature and of the corresponding emission measure, as we would do with real data. We can then construct the trajectory in an equivalent $\overline{n}$-$T$ diagram, where the density is replaced by the square root of the emission measure ($\epsilon^{1/2}$, where $\epsilon = \mathscr{A} \int_0^{s_{max}} n^2 ds$ ), since the coronal volume does not change drastically.

As an example we show in Fig. 1 the light curve and the trajectory in the $\overline{n}$-$T$ diagram for the decay of a flaring model loop with semilength $L = 2 \times 10^9$ cm, maximum temperature $T = 2 \times 10^7$ K, and no heating during the decay ($\tau_H = 0$). The quantities relevant for the analysis described in Sect. 3.1 are the light curve decay time and the slope of the trajectory. We define the light curve decay time $\tau_{LC}$ as the time taken by the count rate in the Al 11.4 $\mu$m filter band to decrease by $1/e$ from the maximum value. The slope $\zeta$ is computed with a linear regression on the trajectory from the maximum of the emission measure down to the point at which the count rate in the Al 11.4 $\mu$m filter band is 1/10 of the maximum value.

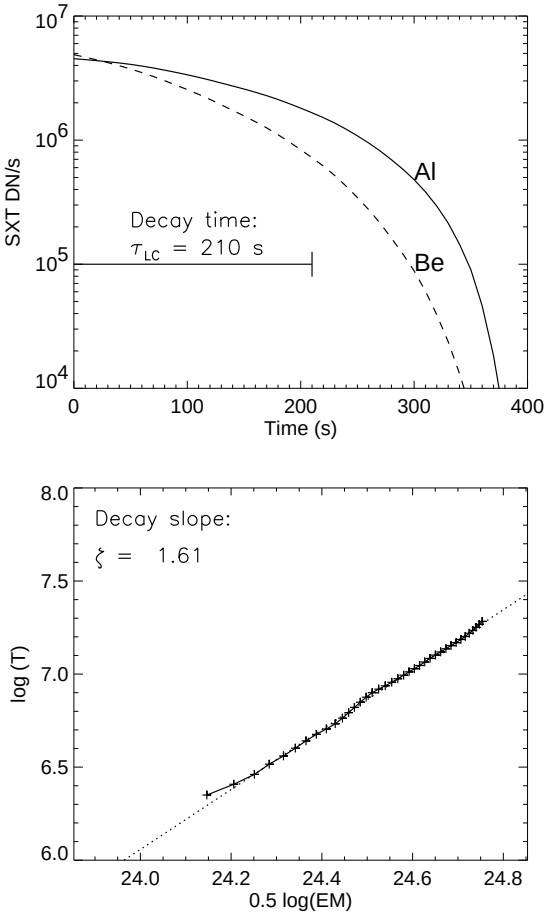


**Fig. 1.** Yohkoh/SXT light curves (*upper panel*) and trajectory in the $\sqrt{\epsilon} - T$ diagram (*lower panel*) of the decay of a model flaring loop with semilength $L = 2 \times 10^9$ cm, maximum temperature $T = 2 \times 10^7$ K, and no heating during the decay ($\tau_H = 0$). The light curves are synthesized in the band of the two hardest SXT filters (Be 119 $\mu$m and Al 11.4 $\mu$m), typically used for flare observations. The horizontal line marks the e-folding decay time $\tau_{LC}$ of the light curve in the Al 11.4 $\mu$m filter band. Temperature and emission measure are derived from the filter ratio, applying the standard Yohkoh analysis. A best fit (*dashed*) line is also drawn, and its slope ($\zeta$) is also shown.

## 3. The derivation of the flare loop length

### *3.1. The method*

The key point of our approach is to use the slope of the trajectory in the $\overline{n}$-$T$ diagram to characterize the effect of the decaying heating on the flare light curve, separating it from the spontaneous thermodynamic decay of the loop (Serio et al. 1991). To this end, we use the results of a set of hydrodynamic simulations of the decay of single flaring loops, as described in the previous section, with various lengths and heating decay times. We are interested in the decay time of the synthesized light curve, which is related to the heating decay time, vs the slope of the trajectory in the effective $\overline{n}$-$T$ diagram, a quantity that we can measure directly from observations even with moderate spectral information. In order to separate the effect of the heating from the spontaneous loop decay in the light curve, the light curve decay time $\tau_{LC}$, as derived from hydrodynamic calculations, is normalized to the spontaneous thermodynamic loop decay time (Serio et al. 1991):

$$\tau_{th} = \alpha L / \sqrt{T} \quad (2)$$

where $\alpha = 3.7 \times 10^{-4}$ cm$^{-1}$ s K$^{1/2}$, $L$ is the loop half-length (cm), and $T$ is the flare maximum temperature (K).

We consider the results of ten model solar flaring loop decays, nine at maximum temperature at the loop apex $T = 2 \times 10^7$ K, five of which with half length $L = 2 \times 10^9$ cm and heating decay times $\tau_H = 0, 1, 2, 4$, and 6 $\tau_{th}$), and the other four with half length $L = 10^{10}$ cm and heating decay times $\tau_H = 0, 1, 2$, and 4 $\tau_{th}$. The tenth model is at maximum temperature $T = 3 \times 10^7$ K, with $L = 2 \times 10^9$ cm and $\tau_H = 0$. Results are shown in Fig. 2, where $\tau_{LC}/\tau_{th}$ is plotted vs the slope $\zeta$ in the $\overline{n}$-$T$ diagram for

[2] The standard Yohkoh SXT functions (Tsuneta et al. 1991) have been adopted.

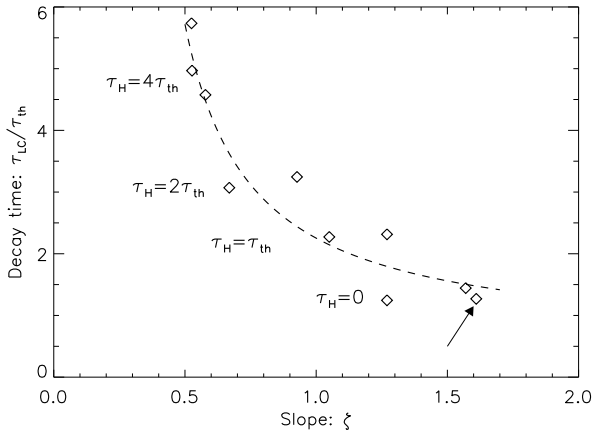


**Fig. 2.** Decay time of synthesized SXT light curves in the Al 11.4 $\mu$m filter band vs slope $\zeta$ in the $\sqrt{\epsilon}-T$ diagram (as of Fig. 1) for models with loop half-length $2\times10^9$ cm and $10^{10}$ cm and heating decay times $\tau_H$, as shown in figure. $T = 2\times10^7$ K for all the models but one ($T = 3\times10^7$ K). The *arrow* points to the model shown in Fig. 1. We also show the function (3) (*dashed*) which we use to fit the model results.

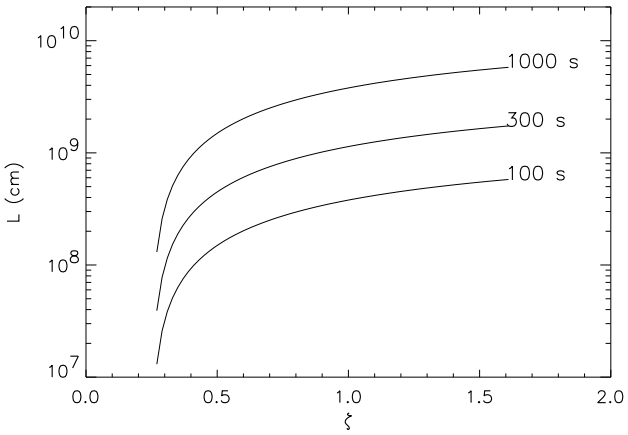


**Fig. 3.** Loop half-length – as derived from Eq. (4) – vs slope, for three different values of the decay time of the SXT light curve.

the nine models above. The models with $\tau_H = 0$ are grouped on the low right hand side. The effect of heating during the decay phase ($\tau_H \neq 0$) is to decrease the slope $\zeta$ and increase the ratio $\tau_{LC}/\tau_{th}$.

We then fit our results by means of an empirical function linking the decay time to the slope. We choose the functional form which satisfies two asymptotic conditions: for very slow decay we expect $\zeta$ to approach a limiting value ($\zeta \sim 0.5$) corresponding to the locus of static loops in the $\overline{n}$-$T$ diagram (cf. Jakimiec et al. 1992); at the other extreme, when the heating is shut off abruptly, the decay time should approach the thermodynamic decay time, i.e. $\tau_{LC}/\tau_{th} \sim 1$. Therefore we suggest the expression in the form of a hyperbolic function:

$$\tau_{LC}/\tau_{th} = \frac{c_a}{\zeta/\zeta_a - 1} + q_a = F(\zeta) \tag{3}$$

to fit the results, with $c_a$, $\zeta_a$ and $q_a$ parameters determined with a non-linear fitting procedure, based on a gradient expansion algorithm, conservatively associating an error $\Delta(\tau_{LC}/\tau_{th}) = 0.1$ on each data point. Fig. 2 shows the resulting function with the following parameters:

$$c_a = 5.4 \pm 1.5 \qquad \zeta_a = 0.25 \pm 0.04 \qquad q_a = 0.52 \pm 0.16$$

obtained with the best-fit procedure on the model results for flares observable with Yohkoh/SXT.

Inverting Eq. (2) and using Eq. (3), we obtain the expression for $L$:

$$L = \frac{\tau_{LC}\sqrt{T}}{\alpha F(\zeta)} \tag{4}$$

The loop length is still proportional to the characteristic decay time, but, in the presence of significant heating during the decay, the denominator becomes large, and the length is reduced, as it should be.

As an aside, once the loop length is determined from Eq. (4), it is straightforward to obtain the heating decay time: the characteristic time $\tau_{th}$ and the ratio $\tau_{LC}/\tau_{th}$ are in fact known, and we can identify the appropriate $\zeta$ value in the plane of Fig. 2, and therefore estimate the heating decay time.

### *3.2. Sensitivity, validity and restrictions*

Eq. (4) has been derived in the hypothesis that model assumptions are valid: flares occurring in semi-circular loops with constant cross-section, whose geometry does not vary significantly during the decay, with exponentially decaying heating and decaying from quasi-stationary conditions. Deviations from these assumptions may affect the predictions of Eq. (4).

Most flares are observed to involve multiple loop structures, which makes the identification of the proper loop length difficult. However we have verified that Eq. (4) generally provides lengths consistent with the linear sizes of such flaring regions. Significant volume variations can render the identification of the linear size ambiguous, but we have noticed that the Eq. (4) still provides reliable results on the dimensions of the longest-lived structure.

Another source of uncertainty is introduced by the scattering of the model results in Fig. 2 and by the fitting procedure, with the consequent uncertainty in the parameters $c_a$, $q_a$ and $\zeta_a$.

Apart from model considerations, we can outline some general guidelines to apply our approach. From Fig. 2 we note that for low values of $\zeta$ a small indetermination in the value of $\zeta$ causes a large indetermination in the ratio $\tau_{LC}/\tau_{th}$, and, as a consequence, in the length estimation. In other words, the prediction of loop length is unreliable for very low values of $\zeta$. This problem is clear in Fig. 3 where the value of loop length is shown vs the slope $\zeta$, for three values of the SXT light curve e-folding time. It is clear that for $\zeta \lesssim 0.3$ the length value is much

affected by small variations of $\zeta$. We operatively set $\zeta \approx 0.3$ as a lower limit for the applicability of Eq. (4)[3].

Another source of uncertainty is the definition of the decay curves as derived from observations. The light curve may present significant deviations from a pure exponential. Also the trajectory of the decay in the $\overline{n}$-$T$ diagram may be badly defined. The slope is derived with a linear regression in the log($\overline{n}$)-log($T$) plane, which may be unreliable either if the trajectory is not linear, or if it is too short to exhibit a well-defined trend. We have ascertained from the tests that results are correct as long as the trajectory in the $\overline{n}$-$T$ diagram is linear and the light curve does not deviate much from an exponential decay.

Another condition for the validity of Eq. (4) is that the loop length is smaller than the flare pressure scale height: this is, indeed, the case for most observed solar flares. It has been shown (Reale et al. 1993) that the decay of long loops is characterized by a smaller $\zeta$, even in the absence of heating. It will be shown in a forthcoming paper that, in the case of such large flaring structures, an expression with parameters different from those of Eq. (4) has to be devised.

We can summarize the conditions of validity of Eq. (4) as follows:

**A)** slope $\zeta \geq 0.3$;
**B)** exponential decay of the light curve;
**C)** well defined linear trajectory of the decay in the $n$-$T$ diagram;
**D)** loop length smaller than the pressure scale height.

The first selection of the test flares in the following section has been done on the basis of the first condition only.

## 4. Testing

### *4.1. Self-consistency*

A necessary (but not sufficient) condition for the validity of Eq. (4) is to reproduce the lengths of the model loops used for its calibration.

In Fig. 4 we show the distribution of the deviations of predicted from true length values $(L_{pred} - L_{true})/L_{true}$ for the models in Fig. 2. All the results, except one, are consistent with the true values within 20%. Although not entirely symmetric, the distribution produced by the assumed function (3) is quite well centered around the zero value (mean 0.01, median 0.004, standard deviation 0.19).

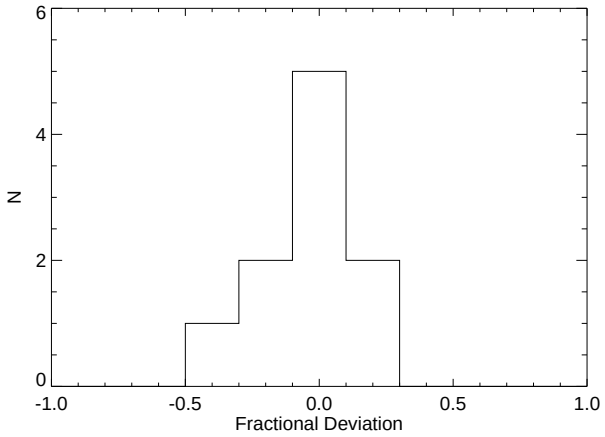


**Fig. 4.** Distribution of $(L_{pred} - L_{true})/L_{true}$ (fractional difference of the predicted and real lengths) for the models in Fig. 2.

### *4.2. Application to Yohkoh/SXT observations*

#### 4.2.1. The analysis

As a test to constrain the effective validity of our approach, we have applied it to solar flare decays monitored with Yohkoh/SXT. From the start of the Yohkoh mission until January 1, 1995, the SXT observed 1261 events in flare mode which had non-zero emission for both the Al 11.4 $\mu$m and Be 119 $\mu$m filters. Of these, 255 flares had decay phases for which the flare mode observations lasted long enough for the SXT emission measure to drop by a factor of 2, 45 of which had SXT and GOES coverage for the entire flare, with single peaks in the emission measure in both instruments. From these 45 flares we have selected 20 flares, between 31 October, 1991 and 2 October 1993 ($\sim$ 2 years), satisfying condition (A) above, i.e. their trajectory in the $n$-$T$ diagram has a slope $\zeta > 0.3$. We relax for the moment the other conditions, which we will discuss while illustrating the results. We only notice now that condition (D) is largely satisfied in all flaring regions.

Flare data obtained from Yohkoh/SXT consist of sequences of images composed by 64×64 pixels of 2.45 arcsec, sampled at a rate of one every few seconds, in the band of selected filters. The images have been processed through the standard SXT processing sequence, including decompression from telemetry data format, background current subtraction, etc. For our analysis, from the SXT data set of each flare we have extracted the light curves in the Be 119 $\mu$m and Al 11.4 $\mu$m filters (the same filters mentioned in Sect. 2), and three images in the Al 11.4 $\mu$m filter band[4]. The light curves are obtained integrating the counts in each frame, and their decay phase has been analysed from the flare maximum until the end of the observing sequence. The three images are taken at the beginning of the observing sequence, i.e. during the rising phase, at the flare maximum and at the end of the observing sequence, i.e. late in the decay phase.

The analysis of the flare data proceeds as follows:

- The light curve decay time is computed as in Sect. 2 (the time taken by the count rate in the Al 11.4 $\mu$m filter band to decrease from the maximum to $1/e$ of the maximum).
- The evolution of temperature and emission measure is obtained from the ratio of the count rates in the two filter bands,

[3] Note that values below this limit are also in contrast with the limiting value $\zeta \sim 0.5$ associated with the locus of the steady-state loops, although this value should be taken only as indicative, since it is derived for plasma density and temperature taken at the top of the model loop, while observed values are representative averages of the emission of the whole loop, filtered through the instrument response.

[4] Be 119 $\mu$m images typically show very similar morphological features.

according to Yohkoh/SXT standard analysis software system (cf. Sect. 2).
- We determine the slope of the trajectory of the $\sqrt{\epsilon} - T$ diagram from the $\epsilon$ maximum to the moment at which the count rate has decreased to 1/10 of the maximum, as is done in the analysis of the model results (Sect. 2), or, if not available, to the last observable minimum of the light curve. The fitting method is a non-weighted linear regression of the data points, with an error provided by the related standard deviation.
- Expression (4) is used to derive the loop size $L$.
- We compare the result to the length measured from a direct inspection of the three images in the Al 11.4 $\mu$m filter band.

#### 4.2.2. The results

The results of the analysis of the light curves are shown in Table 1, where, for each flare, we report the flare maximum temperature, and the slope of the trajectory in the $\overline{n}$-$T$ diagram and its uncertainty, the decay time of the light curve in the Al 11.4 $\mu$m filter band, the loop half-length derived from Eq. (4) using these three quantities, and, for comparison, the scale length derived from Eq. (2), where we have assumed that the decay time $\tau_{th}$ is equal to that of the light curve. As we will discuss in the following, the latter scale length is representative of that derived from other methods of flare loop length estimation. In the last column the inferred heating time scale is shown in units of the natural loop decay time, Eq. (2).

All flares considered have maximum temperature between $7 < \log T < 7.2$. The slopes are in the range $0.32 \leq \zeta \leq 1.27$, the decay times in the range $196 \leq \tau \leq 3740$ sec, and the derived loop half-lengths in the range $0.12 \leq L \leq 20 \times 10^9$ cm, i.e. from very short loops to quite big structures not much smaller than the solar radius (although still much smaller than the local pressure scale height). Most of the loops are not far from $L \approx 10^9$ cm, length typical of active region loops. The slope values $\zeta < 1$ found in most cases (17) indicate the presence of significant heating during the decay (e.g. Jakimiec et al. 1992). This is not uncommon as shown in other flare surveys (Sylwester et al. 1993, McTiernan 1996), but our approach provides also an estimate of the heating time scale; for decay slopes smaller than those of the models shown in Fig. 2, given the large uncertainties in that region, we prefer to quote only a lower limit of the heating time scale.

Now we want to compare the results of this analysis to the dimensions of the structures observed in the SXT images. The identification of flaring loop structures from the X-ray images is non-trivial and, even when successful, the measurement of the loop length can be affected by geometrical projection effects. Therefore we have chosen to compare a projected linear length scale measured from the SXT images to the projected linear loop lengths derived from the models. To this end, in the contour plots of the flare regions, as those shown in Fig. 5, whenever possible, we have identified a pair of bright kernels, approximately located at opposite sides of the flaring structure, and we have operatively defined a linear measured length as the distance between these two kernels. Whenever two kernels could not be identified, we have considered as linear length the largest "diameter" of the 50% level contour, which closely reproduces the distance of the two kernels, when they are identified; using 30% and 70% level contours leads to a change of the linear length estimation of $\sim 25\%$ on the average. In some cases (6, 7, 12, 18) neither of the two methods could be applied, either because the morphology is too complex, or because the morphology evolves and changes significantly during the event. In such cases we quote only roughly estimated values or lower limits. In Fig. 5 contour plots for six representative flaring regions are shown. The linear lengths measured with the two criteria described above are also shown as thick segments, except for flares 6 and 18.

We have compared these measured lengths to the maximum and minimum projected linear loop lengths predicted by the modeling. The maximum length ($L_p^{max}$) is the distance of the loop footpoints when the loop is seen on the disk in its largest extension, while the minimum length ($L_p^{min}$) is the height of the loop, when it is seen edge-on on the limb.

These lengths have computed as:

$$L_p^{min} = \frac{2}{\pi} L_- \qquad\qquad L_p^{max} = \frac{4}{\pi} L_+ \tag{5}$$

where $L_-$ and $L_+$ are the lower and upper values of $L$ obtained by adding the uncertainties of the slope $\zeta$ (we neglect the uncertainties in $\tau$ and $T$).

All these linear lengths are reported in Table 2. A necessary condition for the accordance of the model prediction with the observation is that the linear scale size of the structures in the images $L_p$ is contained in the range between $L_p^{min}$ and $L_p^{max}$.

For ten flares (1 to 5, 10, 14, 15, 17, 20) we could identify the bright kernels. The agreement between the linear lengths is good for six flares, marginal for flares 1, 10 and 15, and bad for flare 17. The very short scale length derived for the region of flare 17 is due to the rapid decay of the light curve. However, if we examine in detail the light curve of this flare we realize that the decay is far from being exponential, but it is first rapid and then slower. The e-folding time is computed on the early phase and it is consequently very short, leading to the short length. The application of condition (B) would have excluded this flare.

For six flares (8, 9, 11, 13, 16 and 19) we derived the length from the 50% level contour and the results of Eq. (4) are consistent with the data for all of them.

As for the other flares, we may hypothesize a coarse agreement for flares 12 and 18 (cf. Fig. 5, panel 6). The length is instead significantly overestimated for flares 6 and 7. Both of them are very long flares and occur in the same active region located on the eastern limb of the solar disk (cf. Fig. 5 panel 3). There are two possible reasons for the inaccurate prediction: i) the trajectory of their decay in the $\overline{n}$-$T$ diagram is quite short ($\Delta \log T \sim 0.2$), so that the resulting slope may be inaccurate; ii) the large structures may be partially occulted by the solar disk, and we may be observing only a fraction of the flaring region, therefore underestimating its size from the images. These two

**Table 1.** Yohkoh SXT flares

| | Flare[a] | log[T (K)] | Slope($\zeta$) | +/- | $\tau_{LC}$(s) | L ($10^9$ cm) | $L_\tau$ ($10^9$ cm) | $\tau_H/\tau_{th}$ |
|---|---|---|---|---|---|---|---|---|
| 1 | 911031.0908 | 7.029 | 0.69 | 0.05 | 501 | 1.3 | 4.3 | 2 |
| 2 | 911102.0644 | 7.135 | 0.62 | 0.05 | 782 | 1.9 | 7.6 | 2-4 |
| 3 | 911218.1024 | 7.104 | 0.78 | 0.11 | 757 | 2.4 | 7.1 | 2 |
| 4 | 911226.2135 | 7.071 | 0.64 | 0.04 | 1030 | 2.5 | 9.3 | 2-4 |
| 5 | 920203.0658 | 7.057 | 0.48 | 0.03 | 574 | 0.9 | 5.1 | 4 |
| 6 | 920206.0316 | 7.117 | 1.27 | 0.14 | 1760 | 10 | 17 | 0-1 |
| 7 | 920206.2051 | 7.138 | 1.16 | 0.13 | 3740 | 19 | 37 | 0-1 |
| 8 | 920209.0301 | 7.022 | 0.47 | 0.05 | 474 | 0.6 | 4.1 | 4 |
| 9 | 920215.2129 | 7.105 | 0.65 | 0.09 | 771 | 2.0 | 7.3 | 2-4 |
| 10 | 920226.0136 | 7.074 | 0.43 | 0.02 | 373 | 0.5 | 3.4 | $\gtrsim$4 |
| 11 | 920704.2246 | 7.082 | 0.34 | 0.11 | 528 | 0.3 | 4.8 | $\gtrsim$4 |
| 12 | 920716.0111 | 6.981 | 0.63 | 0.02 | 368 | 0.8 | 3.0 | 2-4 |
| 13 | 920718.0507 | 7.021 | 0.96 | 0.07 | 245 | 0.9 | 2.1 | 1 |
| 14 | 920811.1347 | 6.985 | 1.20 | 0.06 | 596 | 2.7 | 4.9 | 0-1 |
| 15 | 921019.1753 | 7.045 | 0.65 | 0.01 | 1290 | 3.1 | 11. | 2-4 |
| 16 | 921027.2217 | 6.998 | 0.52 | 0.04 | 690 | 1.1 | 5.7 | 4 |
| 17 | 930210.0734 | 7.049 | 0.32 | 0.02 | 196 | 0.1 | 1.7 | $\gtrsim$4 |
| 18 | 930527.1748 | 7.014 | 0.52 | 0.05 | 926 | 1.5 | 7.8 | 4 |
| 19 | 930927.1207 | 7.063 | 0.55 | 0.05 | 854 | 1.6 | 7.7 | 4 |
| 20 | 931002.0740 | 7.069 | 0.63 | 0.06 | 662 | 1.6 | 6.0 | 2-4 |

[a] The name convention used is the date and time of the beginning of the flare (yymmdd.hhmm).

**Table 2.** Predictions vs data

| | Flare | Data | | Model | |
|---|---|---|---|---|---|
| | | $L_p$($10^9$ cm) | | $L_p^{min}$($10^9$ cm) | $L_p^{max}$($10^9$ cm) |
| 1 | 911031.0908 | 2.1 | a | 0.7 | 1.8 |
| 2 | 911102.0644 | 2.1 | a | 1.1 | 2.7 |
| 3 | 911218.1024 | 2.7 | a | 1.3 | 3.6 |
| 4 | 911226.2135 | 3.3 | a | 1.5 | 3.4 |
| 5 | 920203.0658 | 1.1 | a | 0.5 | 1.2 |
| 6 | 920206.0316 | $\sim$ 4? | c,d | 5.5 | 13 |
| 7 | 920206.2051 | $\sim$ 4? | c,d | 11 | 27 |
| 8 | 920209.0301 | 0.8 | b | 0.3 | 1.0 |
| 9 | 920215.2129 | 2.1 | b | 1.0 | 3.0 |
| 10 | 920226.0136 | 0.8 | a | 0.3 | 0.6 |
| 11 | 920704.2246 | 0.7 | b | 0.0 | 1.0 |
| 12 | 920716.0111 | $>$ 1? | c | 0.5 | 1.0 |
| 13 | 920718.0507 | 0.9 | b | 0.5 | 1.3 |
| 14 | 920811.1347 | 3.0 | a | 1.6 | 3.5 |
| 15 | 921019.1753 | 1.5 | a | 1.9 | 4.0 |
| 16 | 921027.2217 | 0.9 | b | 0.6 | 1.6 |
| 17 | 930210.0734 | 1.4 | a,d | 0.1 | 0.2 |
| 18 | 930527.1748 | $>$ 2? | c | 0.8 | 2.2 |
| 19 | 930927.1207 | 1.3 | b | 0.9 | 2.3 |
| 20 | 931002.0740 | 2.2 | a | 0.9 | 2.0 |

a = distance between bright distant kernels; b = largest diameter of 50% level contour; c = uncertain, due to evolving or very complex morphology; d = largely inconsistent with model predictions.

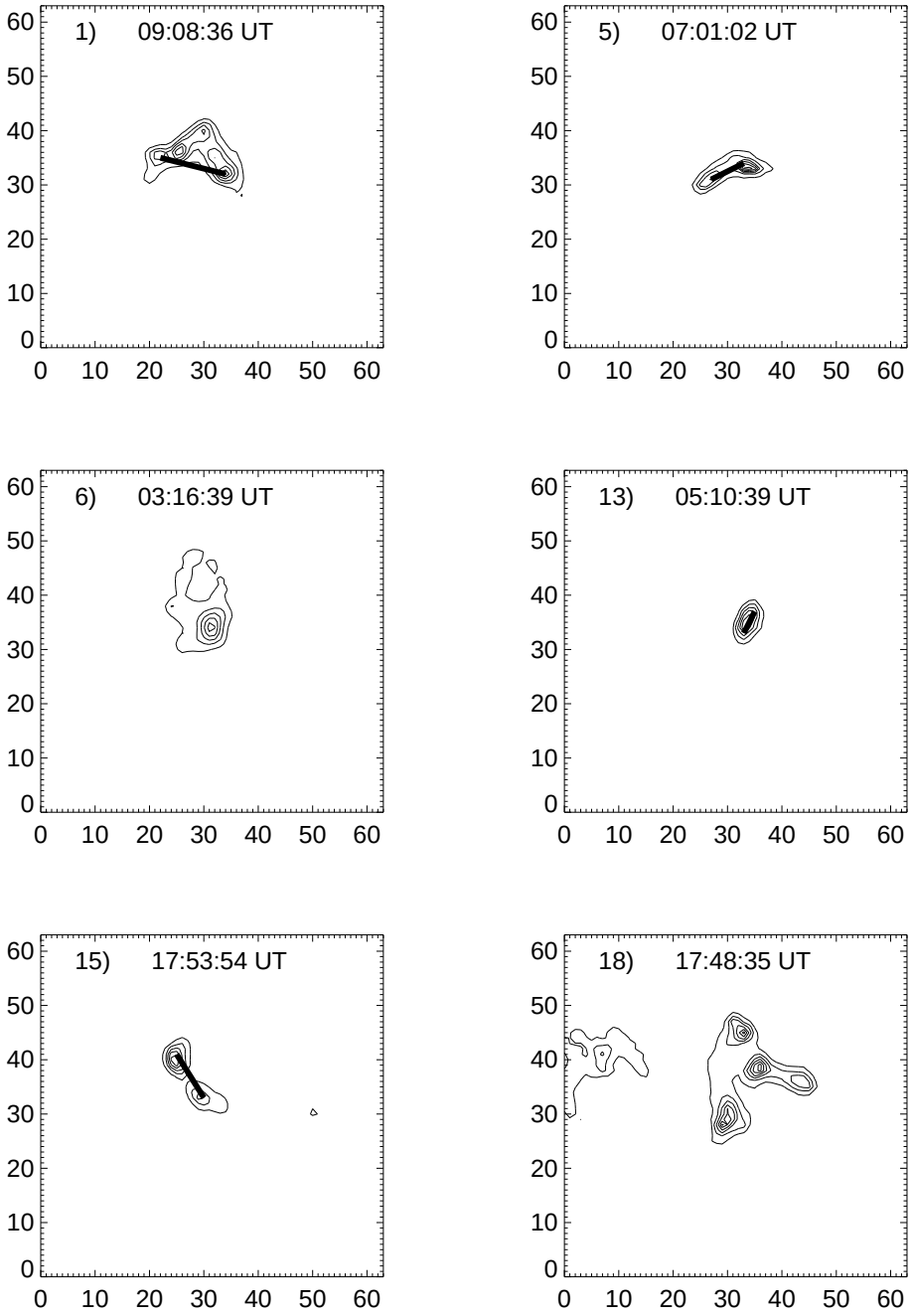


**Fig. 5.** Contour plots of the luminosity in the Al 11.4 $\mu$m filter band, during six representative flares among those in Table 1. Times of the images are labelled. Six linearly equispaced luminosity contours are shown, with a scale normalized to the maximum of each image. The thick lines are the linear scale size in column 3 of Table 2, which could not be identified and, therefore, are not drawn for flares 6 and 18.

flares would have been discarded from the analysis if condition (C) had been applied.

In summary, as shown in Fig. 6, the scale lengths provided by Eq. (4) are consistent, or at worst, in some cases, marginally consistent, with the size of the structures in the images in 17 of 20 flares. A detailed inspection of the three cases of disagreement (6, 7 and 17) has shown that the failure is well motivated, and that more restrictive selection criteria, i.e. a more strict application of conditions (A)-(D), would have rejected these flares.

## 5. Discussion and conclusions

We have devised an expression to derive the geometrical size of flaring regions from the analysis of the flare decay, independently of resolving the structures. The data required for its application are light curves and time-resolved temperature and emission measure values during the decay. The instrument used should therefore have good sensitivity and moderate spectral resolution.

The importance of this approach lies in the fact that, at variance with previous ones, by combining temporal (the light curve) and spectral (the $\overline{n}$-$T$ diagram) information, it takes into proper quantitative account the effect of a prolonged heating

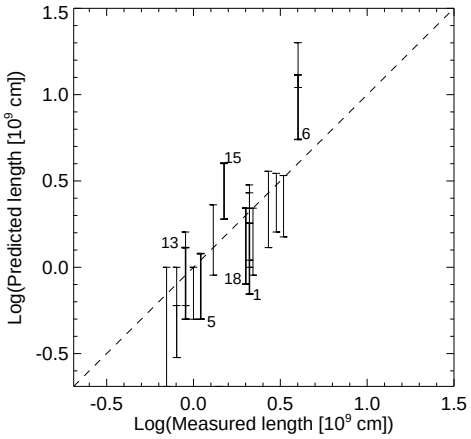


**Fig. 6.** Ranges of expected linear dimensions vs measured linear dimensions of the SXT flares of Table 1. Thick labeled bars mark the flares shown in Fig. 5. Flare 17 is outside the figure range.

during the decay. Comparing columns (7) and (8) in Table 1 helps to evaluate how important the effect of the heating is. Column (8) contains the values of loop half-length derived with Eq.(2), which does not include any effect of the heating. These values are larger by a factor $\sim$ 2 to $\sim$ 10 from those in Column (7), and most of them are clearly unrealistically large when compared to the structures in the SXT images. As shown in Serio et al. (1991) the loop decay time, Eq. (2), is generally shorter than the combination of radiative and conductive cooling times generally used by many authors to estimate stellar flaring loop length, which would lead to still larger and less realistic length values.

Our formula, however, is subject to some restrictions:

1. it is not always applicable, since conditions (A)-(D) in Sect. 3.2 should be satisfied;
2. large uncertainties may result from summing up the uncertainties in the derivation of the Eq. (4) for $L$ to the uncertainties in the observational data, especially when their statistics is low. Therefore there are relatively demanding requirements on the observational data.
3. the basic flare scenario is quite simplified, a single kind of loop with uniform heating, gradual evolution, and constant cross-section. However, as proven by the tests on resolved solar flaring structures, this approach is certainly valid for an analysis of global properties, such as the light curve and the $\overline{n}$-$T$ diagram, and much more refined than previous estimate of unresolved loop lengths.

Even in the light of these limitations, the expression for the loop length yields good results when applied to solar X-ray data collected with Yohkoh/SXT, as shown in Sect. 4.2. The consistency of the predictions with the observed morphology supports the validity of the approach, and, at the same time, confirms the validity of the global approach, including the model assumptions.

This makes us confident for the application of the expression to flares observed with instruments with no angular resolution. Its relatively straightforward applicability makes it particularly appropriate in the systematic analysis of surveys of flares. In this sense our approach has the big advantage of involving the decay phase, which is the most gradual one, and usually the best observed in a flare. In contrast the rising phase is faster, less luminous in the average, and therefore more difficult to observe.

Already the loop length formula could be applied to solar flares observed with non-imaging instruments, such as the Yohkoh Bragg Crystal Spectrometer (BCS), or the GOES instruments, which have collected a very large flare database.

The extensive application to stellar flares observed with telescopes such as ROSAT/PSPC and ASCA/SIS, promises to constrain the dimensions of flaring regions on stars, and to infer the characteristics of the heating during the decay (see Sciortino et al. 1996, for preliminary results). This application requires that the formula is tuned to take into account the spectral responses of these instruments, the low statistics and moderate spectral resolution of stellar data, and the extension to structures of size comparable to the local pressure scale height.

*Acknowledgements.* We thank R. Rosner, R. Pallavicini, G. Micela and S. Sciortino for useful suggestions. We acknowledge partial support from Ministero dell'Università e della Ricerca Scientifica e Tecnologica, Agenzia Spaziale Italiana and Consiglio Nazionale delle Ricerche. Yohkoh data analysis at U. C. Berkeley was supported by Lockheed subcontract SE80D7860R and NASA Grant NAGW-5126.

## References

Betta R. M., Peres G., Reale F., Serio S., 1997, A&AS, 122, 585.
Graffagnino G., Wonnacott D., Schaeidt S., 1995, MNRAS, 275, 129.
Haisch B.M., 1983, in Activity in Red-Dwarf Stars, eds. P.B. Byrne, M. Rodonó, Reidel, Dordrecht, p.255.
Haisch B.M., Antunes A., Schmitt J.H.M.M., 1995, Science, 268, 1327.
Jakimiec J., Sylwester B., Sylwester J., et al. 1992, A&A, 253, 269.
McTiernan J., 1996, Proc. Yohkoh Conference on Observations of Magnetic Reconnection in the Solar Atmosphere, Bath, March 20-22, 1996, B. Bentley, J. Mariska (eds.), in press.
Metcalf T. R., Fisher G. H., 1996, ApJ, 462, 977.
Pallavicini R., Serio S., Vaiana G. S., 1977, ApJ, 216, 108.
Pallavicini R., Peres G., Serio S., et al., 1983, ApJ, 270, 270.
Reale F., Peres G., Serio S., Rosner R., Schmitt J.H.M.M., 1988, ApJ 328, 256.
Reale F., Serio S., Peres G., 1993, A&A, 272, 486.
Reale F., Peres G., 1995, A&A, 299, 225.
Sciortino S., Micela G., Reale F., et al., 1996, Magnetohydrodynamic Phenomena in the Solar Atmosphere - Prototypes of Stellar Magnetic Activity, Y. Uchida et al. (eds.), Kluwer Academic Publishers (Dordrecht), 277.
Serio S., Reale F., Jakimiec J., Sylwester B., Sylwester J., 1991, A&A, 241, 197.
Sylwester B., Sylwester J., Serio S., et al., 1993, A&A, 267, 586.
Tsuneta S., Acton L., Bruner M., et al. 1991, Sol. Phys., 136, 37.
Van den Oord G.H.J., Mewe R., Brinkman A.C., 1988, A&A, 205, 181.

This article was processed by the author using Springer-Verlag LaTeX A&A style file *L-AA* version 3.